Nano Energy 94 (2022) 106926

Contents lists available at ScienceDirect

Nano Energy

journal homepage: www.elsevier.com/locate/nanoen

Highly-stretchable rope-like triboelectric nanogenerator for self-powered monitoring in marine structures

Cong Zhao [a,1], Dehua Liu [a,1], Yawei Wang [a], Zhiyuan Hu [a], Qiqi Zhang [a], Ziyi Zhang [a], Hao Wang [a], Taili Du [a], Yongjiu Zou [a], Haichao Yuan [a], Xinxiang Pan [a,b], Jianchun Mi [a,c], Minyi Xu [a,*]

[a] Dalian Key Lab of Marine Micro/Nano Energy and Self-powered Systems, Marine Engineering College, Dalian Maritime University, Dalian 116026, China
[b] School of Electronics and Information Technology, Guangdong Ocean University, Zhanjiang 524088, China
[c] College of Engineering, Peking University, Beijing 100871, China

ARTICLE INFO

Keywords:
Marine structure monitoring
Self-powered sensor
Rope-like structure
Stretchable sensor
Triboelectric nanogenerator

ABSTRACT

Real-time monitoring in marine structures is vital to prevent maritime accidents. In this study, a highly-stretchable rope-like triboelectric nanogenerator (R-TENG) is proposed and investigated to monitor the mechanical loads of marine structures. The designed R-TENG is composed of outer latex tube and inner silicone rubber core. A series of experiments reveal that the voltage output of the R-TENG increases linearly with the strain in the elastic region of 140%. In addition, the R-TENG can also respond well to other mechanical stimuli such as bending and pressing. More importantly, the electrical output of the R-TENG can remain almost constant even under 93% humidity atmosphere. Finally, the R-TENG has been successfully demonstrated in monitoring the typical mechanical loads in marine structures, including stretching, colliding and bending. Therefore, this R-TENG can be utilized as an alternative sensor to realize the self-powered monitoring in marine structures.

1. Introduction

Marine structures such as offshore platforms and ships play an important role in offshore oil and gas exploitation [1,2]. Marine structures are subject to the harsh ocean environments during the whole operation period [3]. They need to withstand the periodic wave, wind and other risky loads such as storms or accidental collisions [1,4,5]. The chronic exposure to these loads will result in damage or even destruction of the marine structures [6,7]. Marine structure health monitoring is devoted to monitoring various mechanical deformations caused by external loads such as the stretching [8–11], shocking [12–15] and bending [16,17]. Therefore, monitoring in marine structures is necessary to determine the structure safety and predict the residual lifetime [1,18,19].

Up until now, the conventional visual inspection has been still the main method to assess the state of the marine structures [20]. Even though the operators adopt other nondestructive testing methods such as the ultrasonic approach, X-rays and so on, the accuracy of these methods is heavily dependent on the skill and experience of operators. In addition, it is extremely dangerous and inconvenient for the operators to perform examination on the sea, especially under harsh sea conditions. The sensing technology is a promising approach to realize the continuous structure monitoring which is crucial to reduce the inspection cost [21–23]. Among various sensors, optical fiber sensors is considered as a prospective solution in the structure monitoring on observation of their small volume, high accuracy, and anti-electromagnetic interference [1,4,24]. Researchers have adopted optical fiber sensors to monitor the marine structures [4,25–27]. However, as the optical fiber sensor requests continuous external power supply, mainly the batteries, the regular inspection and replacement is needed, which interrupts the continuous monitoring process.

Recently, triboelectric nanogenerator (TENG) has attracted the interest of many researchers due to its excellent performance in self-powered sensing in different fields. The TENG can realize the self-powered sensing by converting the mechanical energy in the environment into the electrical energy to acquire energy independence [28]. Owing to its low cost, a wide range of materials, and great flexibility, TENG has been extensively studied for applications in sensing the

* Corresponding author.
E-mail address: xuminyi@dlmu.edu.cn (M. Xu).
[1] These authors contributed equally to this work.

https://doi.org/10.1016/j.nanoen.2022.106926
Received 9 November 2021; Received in revised form 16 December 2021; Accepted 4 January 2022
Available online 7 January 2022

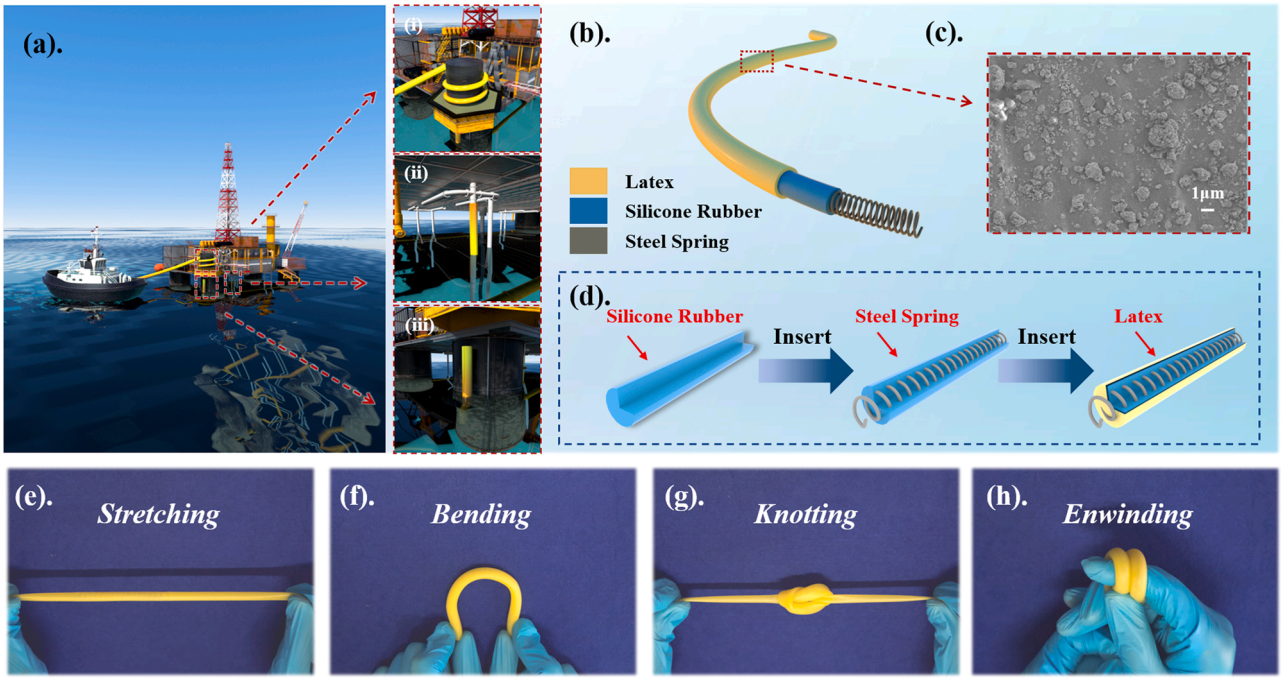

Fig. 1. Application scenario and the structural features of the R-TENG. (a) Application of the R-TENG in marine structure monitoring, including monitoring in (a, i) mooring rope, (a, ii) marine pipeline, (a, iii) platform legs; (b) Structure schematic of the R-TENG; (c) SEM images of latex tube; (d) Fabrication procedures of the R-TENG; Photographs of the R-TENG under (e) stretching, (f) bending, (g) knotting and (h) enwinding state.

vibration [29–31], water level [32–35], angle [36,37], pressure [38–43], sound [44,45] and human motion [46–51]. However, applying TENG to marine structure monitoring is still accompanied by several challenges. Firstly, conventional planar structure is not suitable for the large deformation which the structure and the function may be damaged under the large deformation [52–54]. Besides, the marine structures are exposed to the humid atmosphere while the output performance of TENG is affected seriously by the moisture [55–58]. Thus, the existence of these factors poses a great challenge for the application of TENG in the marine structure monitoring.

In the present study, a highly-stretchable, rope-like triboelectric nanogenerator is proposed as an attractive alternative for self-powered monitoring in marine structures. The designed rope-like TENG (R-TENG) is composed of a highly-elastic latex tube and silicone rubber core as the outer tube and inner core, respectively. Due to the effective combination of structure and material, a series of outstanding characteristics are achieved including the high stretchability, high flexibility and humidity resisting. The electrical output of the R-TENG increases linearly with the increase of strain within 140% elastic strain region. Besides, the R-TENG is also sensitive to other mechanical stimuli including bending and pressing. Furthermore, according to the test results, the R-TENG has good adaptability to high humidity environment. Finally, the present study successfully demonstrates various applications of the R-TENG for real-time monitoring in marine structures, including monitoring of mooring system, platform collision and the bending load. It is believed that our work provides a promising method in the real-time and self-powered monitoring in marine structures.

2. Results and discussion

2.1. Structures and working principle

A schematic diagram of the R-TENG for monitoring the condition of the marine structure, such as the platform and supply vessel, is shown in Fig. 1a. The R-TENG can realize the monitoring in various types of mechanical load including the stretching load exerted on the mooring ropes, the bending load of the marine pipeline and the colliding load acting on the legs of platforms, as shown in Fig. 1a (i-iii). The rope-like structure of the R-TENG makes it easier to deploy on the nonplanar surface of marine structures. The structure schematic of the R-TENG, which is composed of a latex tube and a silicone rubber core with a commercial steel spring inserted inside as the electrode, is shown in Fig. 1b. The Scanning Electron Microscope (SEM) images of the surface morphology is shown in Fig. S1. The latex tube is chosen as the outer tube due to its high flexibility and the composition of the latex tube is shown in Table S1, which is in the supplementary materials. Fig. 1c shows the SEM image of the surface morphology of the latex tube at 1 μm magnification. The nanoparticle structure represents that there is larger specific area on the surface which is helpful to enhance the voltage output [49,50]. As depicted in Fig. 1d, the fabricating process of the R-TENG can be mainly divided into three steps. The silicone rubber core is fabricated through the injection molding technology. Firstly, the liquid silicone rubber is injected into the acrylic mold, and the steel spring is inserted into the liquid silicone rubber. Then, the cured silicone rubber is demolded from the acrylic mold. Finally, the silicone rubber core is inserted into the latex tube (Detailed fabrication process is described in Experimental Section). Thanks to the novel structure design and material selection, the R-TENG exhibits excellent flexibility, which can be seen in Fig. 1e–h, the R-TENG can endure various mechanical deformation such as stretching, bending, knotting and enwinding.

The stiffness constant of the inner silicone rubber core (2.74 N/cm) is much larger than that of the outer latex tube (1.24 N/cm), which means the silicone rubber core to be harder to stretch. As for stretching the R-TENG, the latex is stretched instead of stretching the outer latex tube and the silicone rubber core together. Thus, the stretchability of the R-TENG is mainly determined by the latex tube. As illustrated in Fig. 2a, the R-TENG can be stretched up to 200% owing to the outstanding stretchability of the latex tube, where λ represents the tensile strain. To further study the stretchability of the R-TENG, the tensile force under different strain is investigated. The R-TENG reaches its elastic limit at the 140% tensile strain as indicated in Fig. 2b. In the elastic range of the R-TENG, the tensile force is proportional to the strains, following the formula

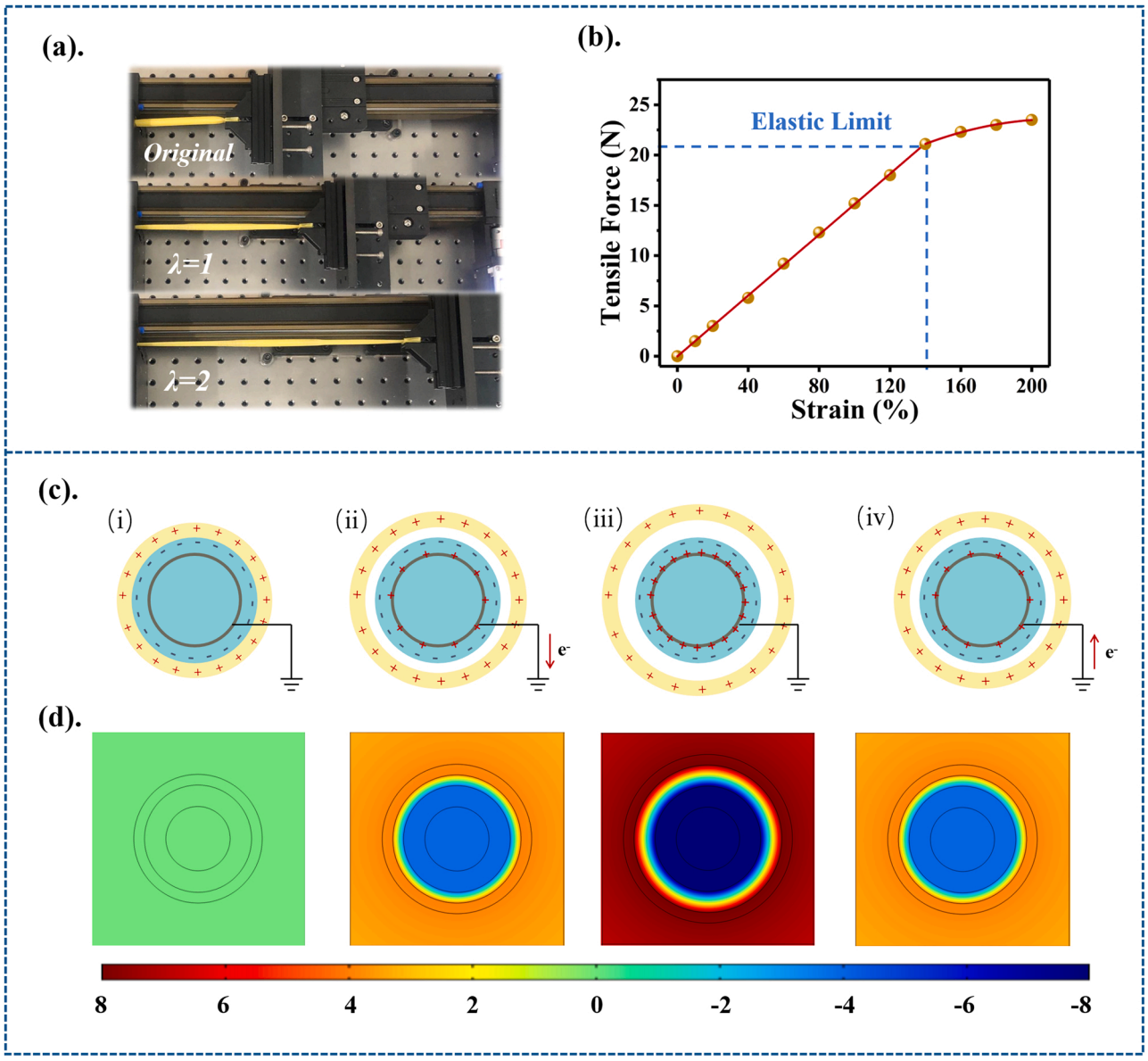

Fig. 2. Tensile behavior and working principle of the R-TENG. Photographs of the R-TENG at (a, i) original state, (a, ii) λ = 1, and (a, iii) λ = 2; (b) Tensile force of the R-TENG under different strain; (c) Working principle of the R-TENG (The cross-section perpendicular to the axial direction is chosen); (d) Potential simulation results by COMSOL.

below:

$$F = k\Delta L = k\lambda H_0 \quad (1)$$

where *F*, *k*, *ΔL* and H_0 represent the tensile force exerted on the R-TENG, stiffness constant, tensile elongation and the length of the R-TENG at the original state, respectively.

The R-TENG works in the single electrode mode. The working principle of the R-TENG is based on the coupling effect of contact electrification and electrostatic induction. As demonstrated in Fig. 2c, the cross-section that perpendicular to axial direction is displayed to show the working principle of the R-TENG. A cycle of stretching-releasing motion can be simplified as a contact-separation process between the outer latex tube and the inner silicone rubber core. In the initial state, as the latex tube is stretched, the surface of inner silicone rubber core contacts with the latex tube in which the negative charges and positive charges are induced respectively due to the electronegativity difference between the two materials, as shown in Fig. 2c (i). It is noted that the accumulated charges will not disappear due to the properties of the insulating polymers even if the separation process occurs [59]. When the latex tube is released, its surface separated from the inner silicone rubber, as indicated in Fig. 2c (ii). The electrons will flow from the steel spring to the ground due to the electrostatic induction effect. Thus, the positive charges will be induced in the electrode. As the gap between the latex tube and the silicone rubber increases furtherly, the transferred charges reach the peak value, which is shown in Fig. 2c (iii). Then, as the stretching process starts again, the electrons flow back to the steel spring from the ground showing in Fig. 2c (iv). Therefore, the periodical tensile force exerted on the R-TENG can produce the alternating electrical current in the external circuit. The working principle proposed above can also be verified through the simulation results of the electrostatic field distribution using the COMSOL Multiphysics software, as depicted in Fig. 2d.

The contact electrification is a key effect for the principle of the R-TENG. An atomic scale electron cloud model [60] is built to express the process of the charge transferring from the latex to silicone rubber, as shown in Fig. S2. When the atoms of the two materials far from each

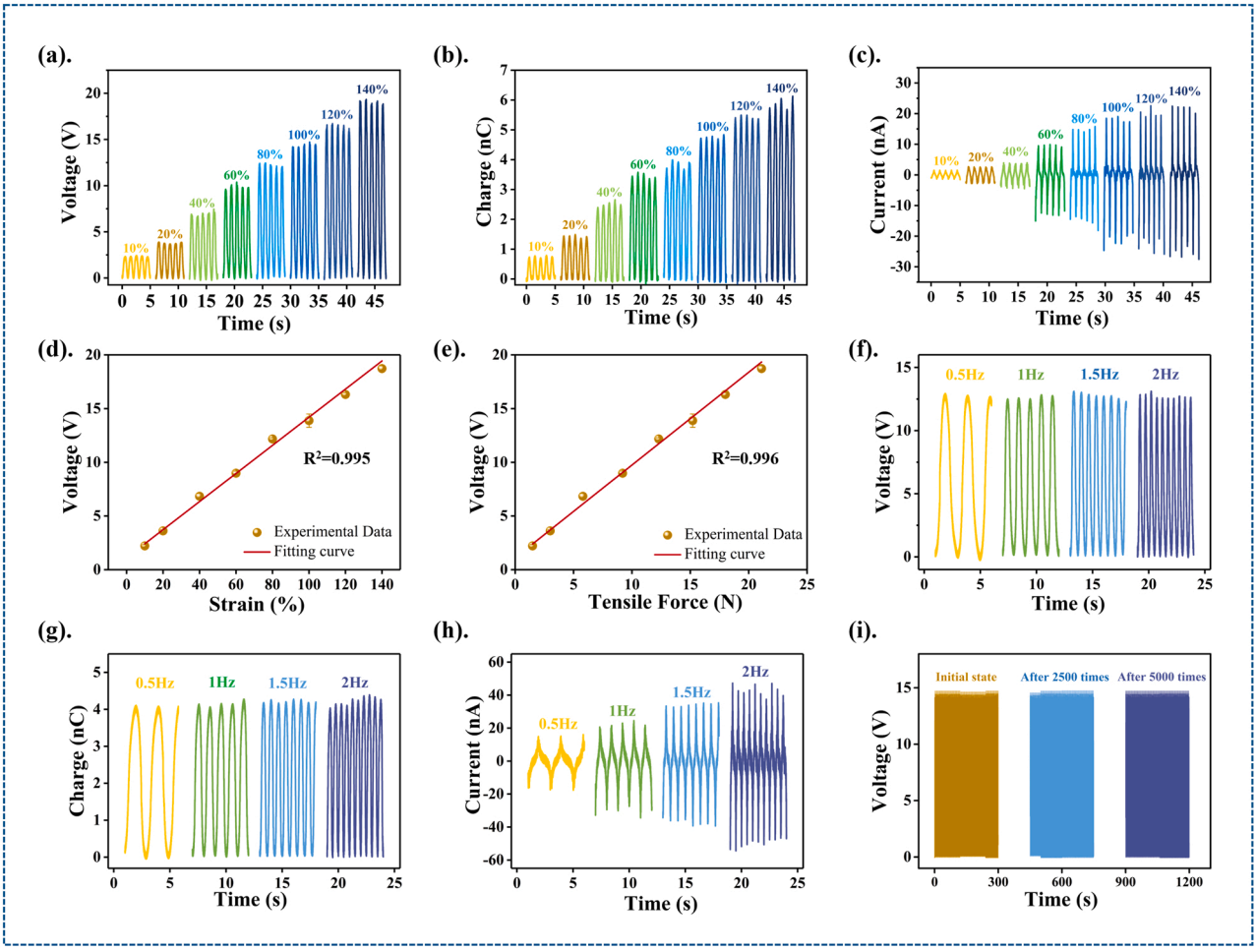

Fig. 3. Electrical output performance of the R-TENG under the stretching state. (a) V_{oc}, (b) Q_{sc}, and (c) I_{sc} of the R-TENG under various strain at the fixed frequency of 1 Hz; The relationships between V_{oc} and (d) strain and (e) tensile force; The output (f) V_{oc}, (g) Q_{sc} and (h) I_{sc} at various frequency under the fixed strain of 80%; (i) The durability of the R-TENG tested for 5000 times under the strain of 100%.

other, there is no overlapping between the two atoms, and they stay in their own orbitals. As the latex tube contacts with the silicone rubber, their electron clouds overlap strongly resulting in the decreasing of the interatomic potential barrier. Under this condition, in order to balance the potential difference between the latex and silicone rubber, the electrons that occupying higher orbits transferred to the empty orbits. After the latex separated from the silicone rubber, the positive charges and negative charges will be maintained in the surface of latex and silicone rubber respectively.

2.2. Performance of the R-TENG

To investigate the electrical output performance of the R-TENG under the stretching state, an alternating tensile force is exerted on the R-TENG through a linear motor, which is one part of the detailed testing system displayed in Fig. S3. On basis of the working principle, the strain and stretching frequency are two main factors related to the output performance of the R-TENG. The influence of strain on the output performance of the R-TENG is investigated with the fixed stretching frequency of 1 Hz and the initial R-TENG length of 100 mm. For testing the performance of the R-TENG as a tensile force sensor, the strain from 10% to 140% is chosen where the tensile force of the R-TENG increases linearly with the strain. As shown in Fig. 3a–c, the open-circuit voltage (V_{oc}), the short-circuit current (I_{sc}) and the short-circuit transferred charge (Q_{sc}) increase from 2.5 V to 20 V, 2 to 25 nA and 0.8 nC to 6 nC respectively as the strain increases from 10% to 140%.

Through further analysis, the relationship between V_{oc} and the strain is investigated as shown in Fig. 3d and the correlation coefficient reaches 0.995 after correlation analysis, which reveals a linear correlation between these two parameters. According to the theory of single-electrode TENG, the voltage output of the R-TENG can be expressed as [61]:

$$V_{oc} = k_q Q_{sc} \quad (2)$$

where k_q is the correlation factor. Therefore, both the theoretical and experimental analysis, Q_{sc} is linearly proportional to the strain of the R-TENG as well as the voltage, and the relationship between Q_{sc} and strain can be seen in Fig. S4. A further possible explanation is that the contacting force between the outer tube and inner core increases as stretching the R-TENG. And the gap between the nanoparticle on the surface (as indicated in Fig. 1d) is fulfilled, leading to the effective contact area increasing between the two surface [62,63], thus increasing Q_{sc}. In addition, Fig. 3e shows there is also a high correlation coefficient of 0.996 between the voltage and the tensile force, which shows the potential of the R-TENG in sensing the tensile force as well. Moreover, the relationship between the electrical output of the R-TENG and the stretching frequency is investigated with the strain of 80%. As the stretching frequency increases from 0.5 Hz to 2 Hz, V_{oc} and Q_{sc} almost remain constant while I_{sc} rises from 14.9 nA to 46.6 nA, see Fig. 3f–h. To verify the robustness of the R-TENG, the durability of the R-TENG is tested and the result is depicted in Fig. 3i. It is demonstrated that a negligible change is observed in the voltage output after 5000

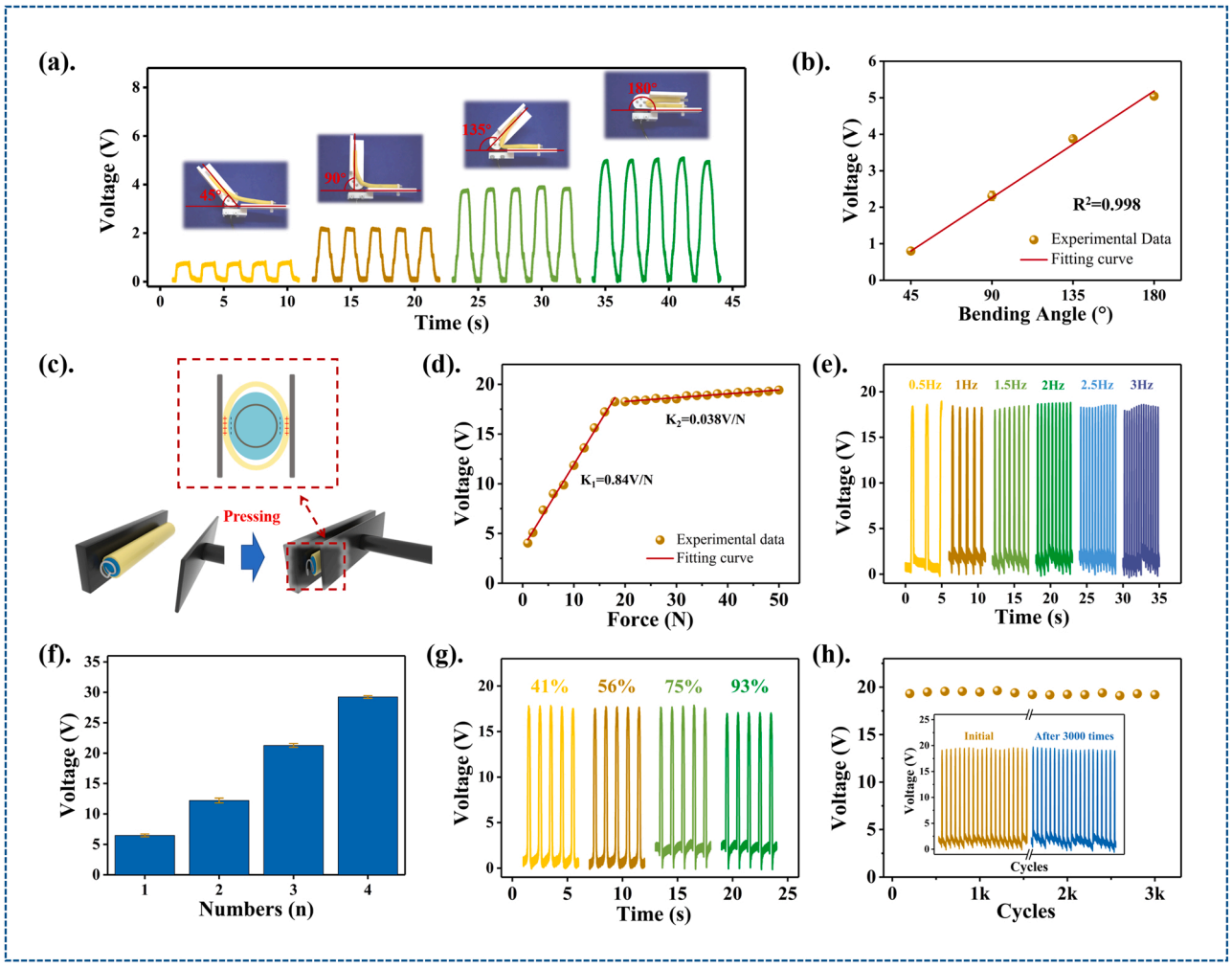

Fig. 4. Electrical output performance of the R-TENG under bending and pressing state. (a) V_{oc} of the R-TENG under various bending angles; (b) Relationship between V_{oc} and the bending angle; (c) Schematic of the R-TENG under the pressing state; (d) V_{oc} of the R-TENG with different pressing force; (e) V_{oc} of the R-TENG with various pressing frequencies; (f) V_{oc} of one to four R-TENGs connecting in parallel; (g) V_{oc} of the R-TENG in different humidity; (h) Durability of the R-TENG tested for 3000 cycles under the pressing force of 18 N.

continuous stretching cycles under 100% strain.

Moreover, the R-TENG also shows good performance in responding to other mechanical stimuli, such as bending and pressing, due to its unique design. As illustrated in Fig. 4a, the dependence of the V_{oc} and the bending angle is investigated and V_{oc} of the R-TENG increases from 0.8 V to 4.8 V with the bending angle increasing from 45° to 180°. This is mainly because the increase of the bending angle results in larger contact area between the outer tube and inner silicone rubber core. Therefore, the R-TENG has the potential to be a self-powered angle sensor due to its high correlation coefficient of 0.998 between the voltage output and bending angle as shown in Fig. 4b.

To explore the electrical output of the R-TENG under the state of pressing, an integral linear motor with pressure feedback control system is deployed. The working mechanism of the R-TENG is displayed in Fig. 4c, the outer tube contacts with the surface of the inner core when exerting the pressing force on the R-TENG resulting in the generation of the positive and negative charges on the two surfaces respectively. As depicted in Fig. 4d, it is noticed that different sensitivity is achieved under different force range. In the force region of 1–18 N, the R-TENG exhibits relatively high sensitivity of 0.84 V/N, while relative low sensitivity of 0.038 V/N in the force region of 18–50 N. The main reason for the different sensitivity in different force range is that the increasing force leads to contacting area change disparately between the outer tube and inner core. When the pressing force is larger than 18 N, the deformation of the silicone rubber core is restricted by the steel spring electrode, contributing to the slow change in contacting area, so as to the smaller variation of voltage output. Fig. 4e shows the V_{oc} almost remains constant at 18.4 V as the pressing frequency increasing from 0.5 Hz to 3 Hz with the pressing force of 18 N, exhibiting the stable output with the same pressing force. Besides, as the number of the R-TENG in parallel is increased from 1 to 4, V_{oc} rises from 6.6 V to 29.3 V under the pressing force of 4 N, as illustrated in Fig. 4f. This represents the ability to meet the high output requirement by the way of array.

More importantly, because of the high humidity at sea, the influence of the humidity on the electrical output performance of the R-TENG is studied. As shown in Fig. 4g, V_{oc} remains almost unchanged even at the 93% humidity indicating that the R-TENG can work in high humidity atmosphere. In addition, for testing the perdurability of the R-TENG, long term output performance test is carried out, as shown in Fig. 4h, even after 3000 times pressing testing (at frequency of 2 Hz, pressing force of 18 N), the R-TENG remains a stable voltage output and the signal curve has no significantly change (see the inset of Fig. 4h) that indicating the good working stability of the R-TENG at the pressing status.

2.3. Demonstration of the R-TENG

The real-time monitoring in the marine structures is vital for

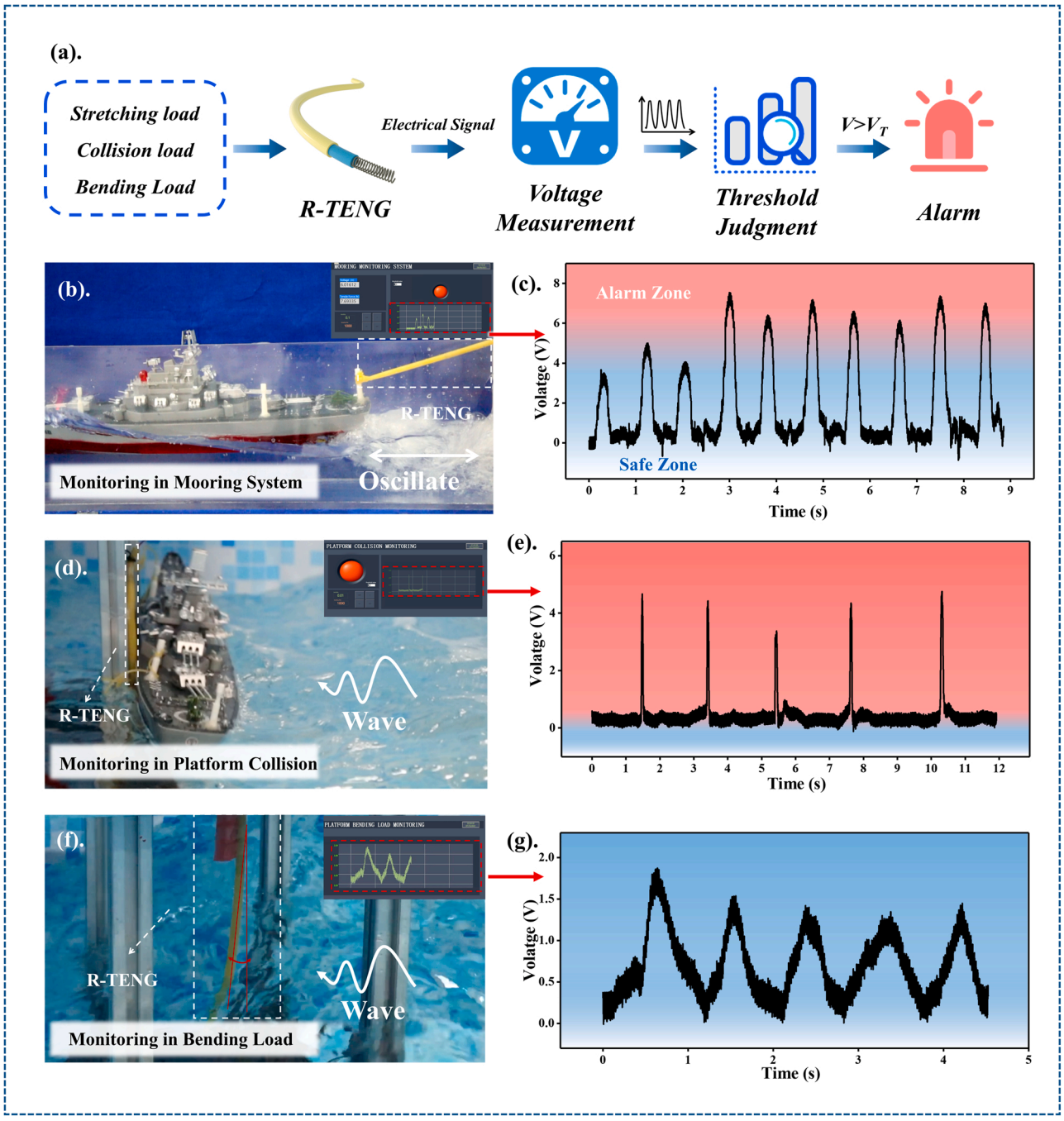

Fig. 5. Demonstration of the R-TENG in monitoring the marine structures. (a) Work flow of the marine structure monitoring system; (b) Image and (c) real-time signal of the R-TENG applied to monitor the mooring system; (d) Image and (e) real-time signal of the R-TENG applied to monitor the collision around platform legs; (f) Image and (g) real-time signal of the R-TENG applied to monitor the bending load of marine pipeline.

preventing the accident resulting from the structural damage over time. Various mechanical loads including stretching, colliding and bending load may act on the marine structures, which need to be monitored. Fig. 5a shows the work flow of the marine monitoring system, in which the R-TENG is used in sensing different mechanical loads. The electrical signal generated by the R-TENG is transmitted to the voltage measurement device, and then an alarm signal will be triggered and delivered if the voltage exceeds the threshold value. In a similar manner, the applications of the R-TENG in monitoring the mooring system, platform collision and bending load are demonstrated in Fig. 5b, d and f, respectively.

As overload is a deterministic cause for the breaking of the mooring rope, the real-time monitoring in the mooring rope status (to ensure the tensile force in the safe zone) is essential to avoid the occurrence of the mooring rope broken accidents. Fig. 5b shows the image of the R-TENG installed on the side of the ship model. The oscillating of the ship model leads to the alternating stretching and releasing of the mooring rope made by the R-TENG. The program and interface of the monitoring is built through the LABVIEW software, as depicted in the inset of Fig. 5b. Fig. 5c shows the electrical signal of the R-TENG during the monitoring process that larger tensile force exerted on the R-TENG results in larger signal peak. As the instantaneous value of the signal exceeds the threshold value (such as 6 V), the alarm indicator will be activated (see Supplementary Movie 1).

Supplementary material related to this article can be found online at doi:10.1016/j.nanoen.2022.106926.

Another scenario depicts the occasional collision between the supply vessel and the platform, which is quite inevitable during the vessel oscillation, and threatens the safety of the vessel and the platform. The R-TENG is deployed on the leg of the platform model to test the performance in monitoring the collisions, as illustrated in Fig. 5d. The real-time signal of the collision is shown in Fig. 5e. It can be seen that every single peak of the signal indicates the occurrence of one collision. And the alarm light shows that the severe collision will be triggered after the voltage exceeds the threshold (such as 2 V), also see Supplementary Movie 2.

Supplementary material related to this article can be found online at doi:10.1016/j.nanoen.2022.106926.

The marine pipelines are important parts of the offshore structures which undertake the task of underwater oil and gas transportation. However, the pipelines are subjected to the water wave resulting in the bending deformation. Fatigue failure may occur over time. Thus, the real-time monitoring in the bending load is vital for preventing the occurrence of the failure. The present R-TENG, as shown in Fig. 5g and Supplementary Movie 3, is fixed in the red tube of the platform model and exhibits good performance in monitoring the bending load of the platform. The demonstration shows the potential of the R-TENG in monitoring the bending load of the marine structures.

Supplementary material related to this article can be found online at doi:10.1016/j.nanoen.2022.106926.

Based on the test above, the R-TENG has successfully demonstrated the applicability in monitoring various mechanical loads, and different signal characteristics are exhibited under different kinds of mechanical load. More importantly, the R-TENG exhibits excellent reliability during the whole working process, even when it completely exposes in the water environment. Therefore, the R-TENG shows its enormous potential in practical application.

3. Conclusion

The present study has proposed a highly stretchable, flexible and self-powered triboelectric nanogenerator for marine structure monitoring. The rope-like TENG is well designed considering the actual application scenario, and composed of the outer latex tube and inner silicone rubber core with the steel spring inserted inside as the electrode. Due to the high elasticity of the latex tube, the voltage output of the R-TENG increases linearly with the strain ratio in the 140% elastic region. In addition, the R-TENG performs well in responding to bending and pressing stimuli. The R-TENG exhibits the sensitivity of 0.84 V/N and 0.038 V/N in the low force region and high force region, respectively. In particular, it is noticed that R-TENG performs well even at 93% humidity atmosphere. Finally, the R-TENG has been successfully demonstrated in monitoring various loads, including mooring rope, collision between ship and platform, and bending of the marine pipelines. This work has provided a promising way to realize the real-time monitoring in the marine structure, so as to achieve a safer marine environment.

4. Experimental section

4.1. Preparation of the R-TENG

For the design of R-TENG, a medical latex tube and the silicone rubber (Ecoflex 00–20) are chosen as the two dielectric layers. The inner core of the R-TENG is made through the injection molding technology. Firstly, the base and curing agent is evenly mixed in a volume ratio of 1:1. Then, the mixture is injected into the column mold with the length of 100 mm and inner diameter of 5 mm. A steel spring is inserted in the mixture before it is cured. Then the silicone rubber is curing at room temperature. The curing silicone rubber is removed from the mold. Finally, the entire silicone rubber is installed in a latex tube with the length of 100 mm, outer diameter of 9 mm, and inner diameter of 6 mm, respectively. Finally, the two ends of the R-TENG are sealed totally through ribbons to prevent the triboelectric layers from contacting with the humidity atmosphere and the water.

4.2. Electrical measurement of the R-TENG

The surface morphology of the latex and silicone rubber is characterized by field emission SEM (Zeiss xrd D8 advance, Germany). When measuring the electrical output of the R-TENG under the state of stretching, the device is mounted on a linear motor (Linmot E1100), the displacement and frequency of which can be adjusted precisely. An apparatus composed of the steering machine and acrylic mold is built for studying the performance of the R-TENG under the bending state. The acrylic mold and the steering machine are connected through screws. An Arduino is used to adjust the bending angle of the device. For measuring the output of the R-TENG under the state of pressing, an integral linear motor with pressure feedback control system (R-LP3) is implemented. The output signals including the open-circuit voltage, short-circuit current and transferred charges are measured by Keithley 6514 electrometer.

CRediT authorship contribution statement

Cong Zhao: Conceptualization, Methodology, Writing – original draft. **Dehua Liu:** Formal analysis, Data curation, Writing. **Yawei Wang:** Figure drawing, Performing the demonstration. **Zhiyuan Hu:** Software. **Qiqi Zhang:** Performing the demonstration. **Ziyi Zhang:** Performing experiments. **Hao Wang:** Writing, Review. **Taili Du:** Providing the suggestion on experiments. **Yongjiu Zou:** Providing the suggestion on experiments. **Haichao Yuan:** Providing the suggestion on experiments. **Xinxiang Pan:** Funding acquisition. **Jianchun Mi:** Writing – review & editing. **Minyi Xu:** Supervision, Writing – review & editing.

Declaration of Competing Interest

The authors declare that they have no known competing financial interests or personal relationships that could have appeared to influence the work reported in this paper.

Acknowledgments

The work was supported by the National Key R & D Project from Ministry of Science and Technology (2021YFA1201604), the National Natural Science Foundation of China (Grant Nos. 51879022, 51979045, 52101400, 52101382, 52101345), Dalian Outstanding Young Scientific and Technological Talents Project (2021RJ11), Innovation Group Project of Southern Marine Science and Engineering Guangdong Laboratory (Zhuhai) (No. 311021013).

Appendix A. Supplementary material

Supplementary data associated with this article can be found in the online version at doi:10.1016/j.nanoen.2022.106926.

References

[1] T. Wang, Z. Yuan, Y. Gong, Y. Wu, Y. Rao, L. Wei, P. Guo, J. Wang, F. Wan, Fiber bragg grating strain sensors for marine engineering, Photon. Sens. 3 (2013) 267–271, https://doi.org/10.1007/s13320-013-0123-6.

[2] W. Cui, F. Wang, X. Huang, A unified fatigue life prediction method for marine structures, Mar. Struct. 24 (2011) 153–181, https://doi.org/10.1016/j.marstruc.2011.02.007.

[3] X. Song, S. Wang, A novel spectral moments equivalence based lumping block method for efficient estimation of offshore structural fatigue damage, Int. J. Fatigue 118 (2019) 162–175, https://doi.org/10.1016/j.ijfatigue.2018.09.016.

[4] L. Ren, Health monitoring system for offshore platform with fiber Bragg grating sensors, Opt. Eng. 45 (2006), 084401, https://doi.org/10.1117/1.2335858.

[5] J.M. Nichols, Structural health monitoring of offshore structures using ambient excitation, Appl. Ocean Res. 25 (2003) 101–114, https://doi.org/10.1016/j.apor.2003.08.003.

[6] B. Kim, C. Min, H. Kim, S. Cho, J. Oh, S.H. Ha, J.H. Yi, Structural health monitoring with sensor data and cosine similarity for multi-damages, Sensors 19 (2019), https://doi.org/10.3390/s19143047.

[7] S. Sony, S. Laventure, A. Sadhu, A literature review of next-generation smart sensing technology in structural health monitoring, Struct. Control Health Monit. 26 (2019) 1–22, https://doi.org/10.1002/stc.2321.

[8] S.W. Lee, K. Sasa, S.-ich Aoki, K. Yamamoto, C. Chen, New evaluation of ship mooring with friction effects on mooring rope and cost-benefit estimation to improve port safety, Int. J. Nav. Archit. Ocean Eng. 13 (2021) 306–320, https://doi.org/10.1016/j.ijnaoe.2021.04.002.

[9] M. López, G. Iglesias, Long wave effects on a vessel at berth, Appl. Ocean Res. 47 (2014) 63–72, https://doi.org/10.1016/j.apor.2014.03.008.

[10] S. Valet, G. Piskoty, S. Michel, C. Affolter, M. Beer, Accident caused by dynamic overloading of a ship mooring rope, Eng. Fail. Anal. 35 (2013) 439–453, https://doi.org/10.1016/j.engfailanal.2013.03.027.

[11] R. Villa-Caro, J.C. Carral, J.Á. Fraguela, M. López, L. Carral, A review of ship mooring systems, Brodogradnja 69 (2018) 123–149, https://doi.org/10.21278/brod69108.

[12] M.P. Mujeeb-Ahmed, S.T. Ince, J.K. Paik, Computational models for the structural crashworthiness analysis of a fixed-type offshore platform in collisions with an offshore supply vessel, Thin-Walled Struct. 154 (2020), 106868, https://doi.org/10.1016/j.tws.2020.106868.

[13] M.P. Mujeeb-Ahmed, J.K. Paik, Quantitative collision risk assessment of a fixed-type offshore platform with an offshore supply vessel, Structures 29 (2021) 2139–2161, https://doi.org/10.1016/j.istruc.2020.06.026.

[14] S. Zhang, P.T. Pedersen, H. Ocakli, Collisions damage assessment of ships and jack-up rigs, Ships Offshore Struct. 10 (2015) 470–478, https://doi.org/10.1080/17445302.2014.1003173.

[15] M.P. Mujeeb-Ahmed, J.K. Seo, J.K. Paik, Probabilistic approach for collision risk analysis of powered vessel with offshore platforms, Ocean Eng. 151 (2018) 206–221, https://doi.org/10.1016/j.oceaneng.2018.01.008.

[16] L. Yuan, S. Kyriakides, Hydraulic expansion of lined pipe for offshore pipeline applications, Appl. Ocean Res. 108 (2021), 102523, https://doi.org/10.1016/j.apor.2020.102523.

[17] A.H. Varma, B.W. Russell, B. Wallace, Large-scale rotating bending fatigue tests for offshore pipe connections, Exp. Mech. 37 (1997) 147–153, https://doi.org/10.1007/BF02317851.

[18] A. Abdelgawad, K. Yelamarthi, Internet of things (IoT) platform for structure health monitoring, Wirel. Commun. Mob. Comput. 2017 (2017) 1–10, https://doi.org/10.1155/2017/6560797.

[19] X. Chapeleau, M. Drissi-Habti, T. Tomiyama, Health monitoring, Mater. Eval. 68 (2010) 408–415, https://doi.org/10.1079/9781845939267.0132.

[20] F. Pacheco-Torgal, J.A. Labrincha, M.V. Diamanti, C.P. Yu, H.K. Lee, Biotechnologies and biomimetics for civil engineering, Biotechnol. Biomim. Civ. Eng. (2015) 1–437, https://doi.org/10.1007/978-3-319-09287-4.

[21] S. Chandrasekaran, T. Chithambaram, Health monitoring of tension leg platform using wireless sensor networking: experimental investigations, J. Mar. Sci. Technol. 24 (2019) 60–72, https://doi.org/10.1007/s00773-018-0531-9.

[22] W. Ostachowicz, R. Soman, P. Malinowski, Optimization of sensor placement for structural health monitoring: a review, Struct. Health Monit. 18 (2019) 963–988, https://doi.org/10.1177/1475921719825601.

[23] R. Severino, R. Gomes, M. Alves, P. Sousa, E. Tovar, L.F. Ramos, R. Aguilar, P. B. Lourenço, A. Wireless Sensor, Network platform for structural health monitoring: enabling accurate and synchronized measurements through COTS+ custom-based design, IFAC (2010), https://doi.org/10.3182/20100908-3-PT-3007.00084.

[24] H.C.H. Li, I. Herszberg, C.E. Davis, A.P. Mouritz, S.C. Galea, Health monitoring of marine composite structural joints using fibre optic sensors, Compos. Struct. 75 (2006) 321–327, https://doi.org/10.1016/j.compstruct.2006.04.054.

[25] R. Min, Z. Liu, L. Pereira, C. Yang, Q. Sui, C. Marques, Optical fiber sensing for marine environment and marine structural health monitoring: a review, Opt. Laser Technol. 140 (2021), 107082, https://doi.org/10.1016/j.optlastec.2021.107082.

[26] M. Mieloszyk, W. Ostachowicz, An application of structural health monitoring system based on FBG sensors to offshore wind turbine support structure model, Mar. Struct. 51 (2017) 65–86, https://doi.org/10.1016/j.marstruc.2016.10.006.

[27] G. Rebel, C.R. Chaplin, C. Groves-Kirkby, I.M.L. Ridge, Condition monitoring techniques for fibre mooring ropes, Insight Non-Destr. Test. Cond. Monit. 42 (2000) 384–390.

[28] S. Wang, L. Lin, Z.L. Wang, Triboelectric nanogenerators as self-powered active sensors, Nano Energy 11 (2015) 436–462, https://doi.org/10.1016/j.nanoen.2014.10.034.

[29] S. Li, D. Liu, Z. Zhao, L. Zhou, X. Yin, X. Li, Y. Gao, C. Zhang, Q. Zhang, J. Wang, Z. L. Wang, A fully self-powered vibration monitoring system driven by dual-mode triboelectric nanogenerators, ACS Nano 14 (2020) 2475–2482, https://doi.org/10.1021/acsnano.9b10142.

[30] T. Du, X. Zuo, F. Dong, S. Li, A.E. Mtui, Y. Zou, P. Zhang, J. Zhao, Y. Zhang, P. Sun, M. Xu, A self-powered and highly accurate vibration sensor based on bouncing-ball triboelectric nanogenerator for intelligent ship machinery monitoring, Micromachines 12 (2021) 1–14, https://doi.org/10.3390/mi12020218.

[31] M. Xu, P. Wang, Y.C. Wang, S.L. Zhang, A.C. Wang, C. Zhang, Z. Wang, X. Pan, Z. L. Wang, A soft and robust spring based triboelectric nanogenerator for harvesting arbitrary directional vibration energy and self-powered vibration sensing, Adv. Energy Mater. 8 (2018) 1–9, https://doi.org/10.1002/aenm.201702432.

[32] J. An, Z. Wang, T. Jiang, P. Chen, X. Liang, J. Shao, J. Nie, M. Xu, Z.L. Wang, Reliable mechatronic indicator for self-powered liquid sensing toward smart manufacture and safe transportation, Mater. Today 41 (2020) 10–20, https://doi.org/10.1016/j.mattod.2020.06.003.

[33] C. Zhang, L. Liu, L. Zhou, X. Yin, X. Wei, Y. Hu, Y. Liu, S. Chen, J. Wang, Z.L. Wang, Self-powered sensor for quantifying ocean surface water waves based on triboelectric nanogenerator, ACS Nano 14 (2020) 7092–7100, https://doi.org/10.1021/acsnano.0c01827.

[34] M. Xu, S. Wang, S.L. Zhang, W. Ding, P.T. Kien, C. Wang, Z. Li, X. Pan, Z.L. Wang, A highly-sensitive wave sensor based on liquid-solid interfacing triboelectric nanogenerator for smart marine equipment, Nano Energy 57 (2019) 574–580, https://doi.org/10.1016/j.nanoen.2018.12.041.

[35] X. Zhang, M. Yu, Z. Ma, H. Ouyang, Y. Zou, S.L. Zhang, H. Niu, X. Pan, M. Xu, Z. Li, Z.L. Wang, Self-powered distributed water level sensors based on liquid–solid triboelectric nanogenerators for ship draft detecting, Adv. Funct. Mater. 29 (2019) 1–8, https://doi.org/10.1002/adfm.201900327.

[36] X. Xie, Y. Chen, J. Jiang, J. Li, Y. Yang, Y. Liu, L. Yang, X. Tu, X. Sun, C. Zhao, M. Sun, Z. Wen, Self-powered gyroscope angle sensor based on resistive matching effect of triboelectric nanogenerator, Adv. Mater. Technol. 6 (2021) 1–7, https://doi.org/10.1002/admt.202100797.

[37] Y. Wu, Q. Jing, J. Chen, P. Bai, J. Bai, G. Zhu, Y. Su, Z.L. Wang, A self powered angle measurement sensor based on triboelectric nanogenerator, Adv. Funct. Mater. 25 (2015) 2166–2174, https://doi.org/10.1002/adfm.201403828.

[38] L. Lin, Y. Xie, S. Wang, W. Wu, S. Niu, X. Wen, Z.L. Wang, Triboelectric active sensor array for self-powered static and dynamic pressure detection and tactile imaging, ACS Nano 7 (2013) 8266–8274, https://doi.org/10.1021/nn4037514.

[39] G. Zhu, W.Q. Yang, T. Zhang, Q. Jing, J. Chen, Y.S. Zhou, P. Bai, Z.L. Wang, Self-powered, ultrasensitive, flexible tactile sensors based on contact electrification, Nano Lett. 14 (2014) 3208–3213, https://doi.org/10.1021/nl5005652.

[40] D. Yang, H. Guo, X. Chen, L. Wang, P. Jiang, W. Zhang, L. Zhang, Z.L. Wang, A flexible and wide pressure range triboelectric sensor array for real-time pressure detection and distribution mapping, J. Mater. Chem. A 8 (2020) 23827–23833, https://doi.org/10.1039/d0ta08223f.

[41] H. Lei, J. Xiao, Y. Chen, J. Jiang, R. Xu, Z. Wen, B. Dong, X. Sun, Bamboo-inspired self-powered triboelectric sensor for touch sensing and sitting posture monitoring, Nano Energy 91 (2021), 106670, https://doi.org/10.1016/j.nanoen.2021.106670.

[42] H. Lei, Y. Chen, Z. Gao, Z. Wen, X. Sun, Advances in self-powered triboelectric pressure sensors, J. Mater. Chem. A 9 (2021) 20100–20130, https://doi.org/10.1039/d1ta03505c.

[43] P. Xu, X. Wang, S. Wang, T. Chen, J. Liu, J. Zheng, W. Li, M. Xu, J. Tao, G. Xie, A triboelectric-based artificial whisker for reactive obstacle avoidance and local mapping, Research 2021 (2021) 1–10, https://doi.org/10.34133/2021/9864967.

[44] H. Zhao, X. Xiao, P. Xu, T. Zhao, L. Song, X. Pan, J. Mi, M. Xu, Z.L. Wang, Dual-tube helmholtz resonator-based triboelectric nanogenerator for highly efficient harvesting of acoustic energy, Adv. Energy Mater. 9 (2019) 1–10, https://doi.org/10.1002/aenm.201902824.

[45] C. Chen, Z. Wen, J. Shi, X. Jian, P. Li, J.T.W. Yeow, X. Sun, Micro triboelectric ultrasonic device for acoustic energy transfer and signal communication, Nat. Commun. 11 (2020), https://doi.org/10.1038/s41467-020-17842-w.

[46] T. Zhang, L. Xie, J. Li, Z. Huang, H. Lei, Y. Liu, Z. Wen, Y. Xie, X. Sun, All-in-one self-powered human–machine interaction system for wireless remote telemetry and control of intelligent cars, Nanomaterials 11 (2021) 1–11, https://doi.org/10.3390/nano11102711.

[47] X. Pu, H. Guo, Q. Tang, J. Chen, L. Feng, G. Liu, X. Wang, Y. Xi, C. Hu, Z.L. Wang, Rotation sensing and gesture control of a robot joint via triboelectric quantization sensor, Nano Energy 54 (2018) 453–460, https://doi.org/10.1016/j.nanoen.2018.10.044.

[48] C. Li, D. Liu, C. Xu, Z. Wang, S. Shu, Z. Sun, W. Tang, Z.L. Wang, Sensing of joint and spinal bending or stretching via a retractable and wearable badge reel, Nat. Commun. 12 (2021) 1–11, https://doi.org/10.1038/s41467-021-23207-8.

[49] Y. Zou, P. Tan, B. Shi, H. Ouyang, D. Jiang, Z. Liu, H. Li, M. Yu, C. Wang, X. Qu, L. Zhao, Y. Fan, Z.L. Wang, Z. Li, A bionic stretchable nanogenerator for underwater sensing and energy harvesting, Nat. Commun. 10 (2019) 1–10, https://doi.org/10.1038/s41467-019-10433-4.

[50] J. Wang, S. Li, F. Yi, Y. Zi, J. Lin, X. Wang, Y. Xu, Z.L. Wang, Sustainably powering wearable electronics solely by biomechanical energy, Nat. Commun. 7 (2016) 1–8, https://doi.org/10.1038/ncomms12744.

[51] X. Pu, H. Guo, J. Chen, X. Wang, Y. Xi, C. Hu, Z.L. Wang, Eye motion triggered self-powered mechnosensational communication system using triboelectric nanogenerator, Sci. Adv. 3 (2017) 1–8, https://doi.org/10.1126/sciadv.1700694.

[52] X. He, Y. Zi, H. Guo, H. Zheng, Y. Xi, C. Wu, J. Wang, W. Zhang, C. Lu, Z.L. Wang, A highly stretchable fiber-based triboelectric nanogenerator for self-powered wearable electronics, Adv. Funct. Mater. 27 (2017) 1–8, https://doi.org/10.1002/adfm.201604378.

[53] K. Dong, J. Deng, W. Ding, A.C. Wang, P. Wang, C. Cheng, Y.C. Wang, L. Jin, B. Gu, B. Sun, Z.L. Wang, Versatile core–sheath yarn for sustainable biomechanical energy harvesting and real-time human-interactive sensing, Adv. Energy Mater. 8 (2018) 1–12, https://doi.org/10.1002/aenm.201801114.

[54] J. Han, C. Xu, J. Zhang, N. Xu, Y. Xiong, X. Cao, Y. Liang, L. Zheng, J. Sun, J. Zhai, Q. Sun, Z.L. Wang, Multifunctional coaxial energy fiber toward energy harvesting, storage, and utilization, ACS Nano 15 (2021) 1597–1607, https://doi.org/10.1021/acsnano.0c09146.

[55] K.Y. Lee, J. Chun, J.H. Lee, K.N. Kim, N.R. Kang, J.Y. Kim, M.H. Kim, K.S. Shin, M. K. Gupta, J.M. Baik, S.W. Kim, Hydrophobic sponge structure-based triboelectric nanogenerator, Adv. Mater. 26 (2014) 5037–5042, https://doi.org/10.1002/adma.201401184.

[56] V. Nguyen, R. Zhu, R. Yang, Environmental effects on nanogenerators, Nano Energy 14 (2014) 49–61, https://doi.org/10.1016/j.nanoen.2014.11.049.
[57] M. Xu, Y.C. Wang, S.L. Zhang, W. Ding, J. Cheng, X. He, P. Zhang, Z. Wang, X. Pan, Z.L. Wang, An aeroelastic flutter based triboelectric nanogenerator as a self-powered active wind speed sensor in harsh environment, Extrem. Mech. Lett. 15 (2017) 122–129, https://doi.org/10.1016/j.eml.2017.07.005.
[58] T.H. Chang, Y.W. Peng, C.H. Chen, T.W. Chang, J.M. Wu, J.C. Hwang, J.Y. Gan, Z. H. Lin, Protein-based contact electrification and its uses for mechanical energy harvesting and humidity detecting, Nano Energy 21 (2016) 238–246, https://doi.org/10.1016/j.nanoen.2016.01.017.
[59] F. Saurenbach, D. Wollmann, B.D. Terris, A.F. Diaz, Force microscopy of ion-containing polymer surfaces: morphology and charge structure, Langmuir 8 (1992) 1199–1203, https://doi.org/10.1021/la00040a030.
[60] Z.L. Wang, A.C. Wang, On the origin of contact-electrification, Mater. Today 30 (2019) 34–51, https://doi.org/10.1016/j.mattod.2019.05.016.
[61] Z.L. Wang, L. Lin, Y. Zi, J. Chen, S. Niu, Triboelectric Nanogenerators, Springer, Berlin, 2016.
[62] G. Zhu, Z.H. Lin, Q. Jing, P. Bai, C. Pan, Y. Yang, Y. Zhou, Z.L. Wang, Toward large-scale energy harvesting by a nanoparticle-enhanced triboelectric nanogenerator, Nano Lett. 13 (2013) 847–853, https://doi.org/10.1021/nl4001053.
[63] Y. Zou, J. Xu, K. Chen, J. Chen, Advances in nanostructures for high-performance triboelectric nanogenerators, Adv. Mater. Technol. 6 (2021) 1–16, https://doi.org/10.1002/admt.202000916.

Cong Zhao is currently pursuing his doctor degree in Dalian Maritime University, China. His current research interests include self-powered system, intelligent marine equipment monitoring and triboelectric nanogenerator.

Dehua Liu is currently pursuing the master's degree in Dalian Maritime University, China. His current research direction is the self-powered system of life-saving equipment based on triboelectric nanogenerators.

Yawei Wang is currently pursuing his master degree in Dalian Maritime University,China.His current research interests include triboelectric-nanogenerators and blue energy.

Zhiyuan Hu is currently pursuing the master's degree in Dalian Maritime University, China His current research direction is the Circuit Management and Signal acquirement of triboelectric nanogenerators.

Qiqi Zhang is currently pursuing his master degree in Dalian Maritime University, China. His current research interests include acoustic energy, self-powered systems and triboelectric nanogenerators.

Ziyi Zhang is currently pursuing his master degree in Dalian Maritime University, China. His current research interests in liquid-solid TENG, blue energy and self-powered systems.

Hao Wang received his Ph.D. degree from Texas A&M University. Now he is an associate professor in Marine engineering College, Dalian Maritime University. His research interests include motion simulation, improvement, and stability analysis of the wave energy harvester.

Taili Du received his B.S. and M.S. from Dalian Maritime University in China in 2008 and 2010. Since 2010, he is with Dalian Maritime University where he is currently an Associate Professor. Currently, he is as a doctoral candidate in Marine Engineering College, Dalian Maritime University. His current research work focus on intelligent equipment performance monitoring and self-powered sensor based on Triboelectric Nanogenerator.

Yongjiu Zou is an assistant professor at College of Marine Engineering, Dalian Maritime University. He received his B.S. and M.S. in marine engineering both from Dalian Maritime University in 2012 and 2014, respectively. His research focuses on triboelectric nanogenerators for energy harvesting and self-powered sensors.

Haichao Yuan received his Master's degree in Dalian Maritime University in 2014, he is now working in Dalian Maritime University. He is currently pursuing his doctor degree in Dalian Maritime University, China. His current research interests include energy harvesters, self-powered systems, triboelectric nanogenerators.

Xinxiang Pan received his B.E and Ph.D. degrees from Marine Engineering College, Dalian Maritime University, China, in 1987 and 1999. He now is President of Guangdong Ocean University. His research interests include smart and green ship, ocean engineering, energy saving and emission reduction, ship safety and pollution control, microfluidic chip, nano energy and self-powered systems.

Prof. Jianchun Mi received his Ph.D. degrees from Newcastle University in 1995. He was a national researcher and director researcher of Adelaide University in Australia from 1995 to 2006. He joined Peking University in 2006, and now he is a full professor in the College of Engineering. His research interests include turbulence, combustion and renewable energy.

Minyi Xu received his Ph.D. degree from Peking University in 2012. During 2016–2017, he joined Professor Zhong Lin Wang' group at Georgia Institute of Technology. Now he is a Professor in the Marine Engineering College, Dalian Maritime University. His current research is mainly focused on the areas of blue energy, self-powered systems, triboelectric nanogenerators and its practical applications in smart ship and ocean.